Utility of Hepatic Perivascular Adipose Tissue as a CT Biomarker for Staging Liver Fibrosis

Skylar Chan*, Tejas Sudharshan Mathai*, Sydney V. Lewis*, Anisa V. Prasad*,
Jianfei Liu*, Meghan G. Lubner[†], Perry J. Pickhardt[†], Ronald M. Summers*

* Radiology and Imaging Sciences, National Institutes of Health Clinical Center, Bethesda, MD, USA

[†] Department of Radiology, University of Wisconsin School of Medicine & Public Health, Madison, Wisconsin, USA

Email: tejas dot mathai at nih dot gov

Abstract—**Repeated injury to the liver can cause liver fibrosis with end-stage cirrhosis being the 12th leading cause of death in the United States. Earlier stages of liver fibrosis can be reversed with treatment, but later stages are irreversible. A redistribution of liver segment volume and increase in periportal fat are previously known biomarkers of later fibrosis stages. We hypothesize that perivascular adipose tissue (PVAT) around the hepatic arteries and portal vein may also be predictive of liver fibrosis. In this pilot work, an automated pipeline was developed to segment the liver, spleen, and hepatic vessels on CT. Next, the PVAT around the hepatic arteries and portal vein was identified. Then, imaging-based biomarkers (e.g., volume, attenuation, fat fraction) of the liver, spleen, and PVAT were calculated. The biomarkers were used to train uni- and multivariate logistic regression models to distinguish advanced fibrosis and cirrhosis. On a sample of 480 patients, the best multivariate model for cirrhosis achieved 96.3% AUC with biomarkers of hepatic PVAT, liver and spleen, and without blood serum scores. For advanced fibrosis, the multivariate model obtained 92.2% AUC with features of PVAT, spleen and liver, and serum scores. To our knowledge, we are the first to show that PVAT-based biomarkers may be clinically useful for staging fibrosis.**

Index Terms—**CT, Liver Fibrosis, Cirrhosis, Perivascular Adipose Tissue, Portal Vein, Hepatic Arteries**

I. INTRODUCTION

Liver fibrosis arises from scar tissue buildup due to repeated injury to the liver that can hamper blood flow to the liver. The causes of fibrosis include Hepatitis B or C viral infection, alcohol abuse, and metabolic syndrome-associated steatohepatitis (e.g., due to obesity or diabetes), among others. Chronic liver disease affects ∼4.5 million adults each year [1], and unchecked fibrosis can result in end-stage cirrhosis, which is the 12th leading cause of death in the US. Early intervention and treatment can reverse earlier fibrosis stages, which makes it crucial to differentiate them from later stages (advanced fibrosis and cirrhosis).

Liver biopsy is the gold standard approach for staging fibrosis, but it is invasive and prone to sampling errors. Lab serum tests can also be used, however they are insufficient and cannot replace histology [2]. Thus, non-invasive imaging-based biomarkers that perform better than histology or lab tests are highly sought after [3]. Abdominal contrast-enhanced CT (CECT) is one imaging technique to evaluate liver disease and cirrhosis [2], [4]–[8]. On CT, certain findings clearly indicate liver fibrosis and cirrhosis. These include portal hypertension with splenomegaly or ascites [7]–[9], the redistribution of liver segments [8], variceal hemorrhage [10], and increased nodularity ("bumpiness") of the anterior liver surface [2], [5], [11]–[13]. Imaging-based biomarkers (e.g., volume, attenuation) representing these findings were calculated in prior works and have been utilized for staging fibrosis.

In this paper, we hypothesize that biomarkers of the fat or perivascular adipose tissue (PVAT) surrounding the vessels in the liver (hepatic arteries and portal vein) can also be used to stage fibrosis. To that end, a fully automated deep learning-based pipeline was developed to distinguish advanced fibrosis and cirrhosis from earlier fibrosis stages. PVAT biomarkers and several imaging-based biomarkers from the liver and spleen were automatically computed. Uni- and multi-variate logistic regression models were trained with these biomarkers, and evaluated for their capability to differentiate advanced fibrosis and cirrhosis. To our knowledge, we are the first to examine the utility of peri-vascular fat around the hepatic vessels for staging hepatic fibrosis.

II. METHODS

A. *Patient Sample*

In this retrospective study, 480 patients (304 men, median age: 49 ± 9 years) underwent abdominal contrast-enhanced CT exams at the University of Wisconsin-Madison medical system between 2000 – 2016 [8]. Patients were staged using the METAVIR system and categorized into 3 groups: patients who underwent CT imaging as potential kidney donors without any known symptoms or liver disease (F0, n = 151); patients with variable degrees of pre-cirrhotic hepatic fibrosis including early (F1, n = 52), intermediate (F2, n = 82), and advanced (F3, n = 56) fibrosis; and patients with chronic liver disease (cirrhosis) who had undergone evaluation for liver transplant (F4, n = 139). Multiple CT scanners were used for imaging (GE, Canon and Siemens) with the tube voltage range between 100 - 140 kVp and patient specific tube current settings. Volume dimensions ranged from 512 × 512 × (73 - 482) voxels and the spacing ranged between 2.5 - 5 mm. A liver biopsy within 1 year of the CT exam was required for patients in the early (F1), intermediate (F2), and advanced (F3) fibrosis cohorts. Lab test results (serum AST, ALT, platelet counts, FIB-4 and APRI scores) were also available.
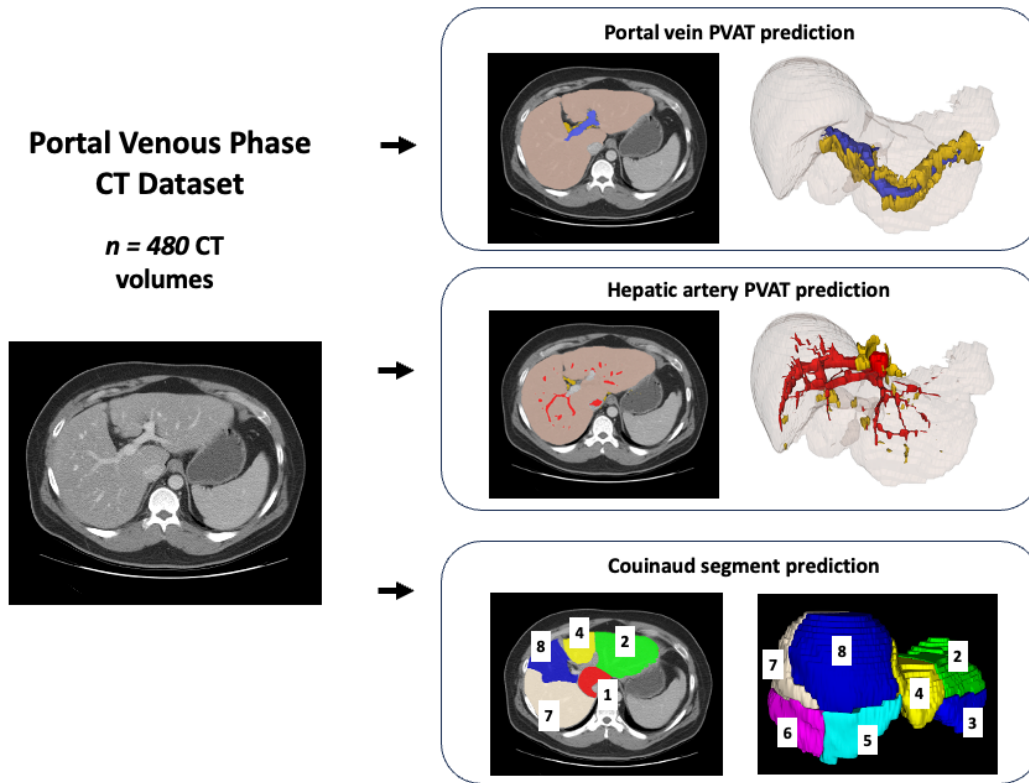
Fig. 1: Automated framework for liver fibrosis staging. Publicly available tools (TotalSegmentator and MSD Task-8 nnU-Net) segmented the liver, spleen, and hepatic vessels. CT biomarkers (volume, attenuation, fat fraction) of the liver, spleen and perivascular adipose tissue (PVAT) were automatically derived. The liver (light brown), Couinaud segments (various colors), portal vein (blue), hepatic veins and arteries (red), PVAT (yellow) can be seen. CT biomarkers were used for staging advanced fibrosis and cirrhosis.

B. Segmentation of Organs, Vasculature, and Body Fat

Organs: Figure 1 shows an overview of the pipeline. Segmentations of the liver and spleen were required to compute biomarkers. First, the public TotalSegmentator (TS) tool [14] was used to segment 117 different structures in the body, from which the liver and spleen segmentations were extracted. Additionally, segmentations of the eight liver Couinaud segments were also obtained using another validated tool [8], [11]–[13].

Vasculature: The vessels feeding the liver include the hepatic artery, the portal vein, and their branches. TS only segments the main portal vein. It does not segment the portal vein branches or other hepatic vessels. To obtain these segmentations, a publicly available nnU-Net model (task 8) trained on the Medical Segmentation Decathlon (MSD) challenge was used [15], [16]. The portal vein segmentation from TS was removed (masked out) from the nnU-Net hepatic vessels segmentation. The purpose was to separate the segmentation of the hepatic arteries from the portal vein, such that biomarkers from each vessel could be computed separately and used for staging liver fibrosis. However, due to segmentation errors (either by TS or nnU-Net), there could be some minor overlap between the two vessel trees.

C. Automated Extraction of Imaging-based Biomarkers

Liver and Spleen Biomarkers: Segmentations of the liver, its Couinaud segments, and spleen were used to compute biomarkers. These included: volume, attenuation (mean and standard deviation), liver segmental volume ratio (LSVR, the volume ratio of liver segments 1-3 to 4-8) [8], and liver surface nodularity (LSN) [11]–[13].

PVAT Biomarkers: The segmentations of the hepatic arteries and portal vein were dilated with a kernel size of 4x4 pixels following prior empirical research [17], [18]. Then, voxels in the dilated region that fell within the HU range of $[-190, -30]$ were identified, and these voxels corresponded to hepatic PVAT. In particular, PVAT around the hepatic arteries was derived from hepatic artery segmentations provided by nnU-Net, while PVAT around the portal vein was derived from portal vein segmentations provided by TS. These PVAT voxels were used to calculate biomarkers including: volume, mean & standard deviation (SD) of CT attenuation, and fat fraction. To account for variations in scanners, acquisition settings, and disease characteristics, the PVAT CT attenuation was normalized by the average vessel lumen attenuation [18].

D. Liver Fibrosis Staging

In this work, we focus on distinguishing advanced fibrosis and cirrhosis stages. Several uni- and multi-variate logistic regression models were built (LR, scikit-learn package, Python v3.12). These models used various combinations of the clinical and automated measurements as features to differentiate advanced fibrosis and cirrhosis (advanced fibrosis group included cirrhosis patients). The dataset was divided into training (80%, n = 385 patients) and testing (20%, n = 95 patients) subsets. The test data subset contained 19 randomly sampled patients from each fibrosis stage. The best univariate features were identified for each model and then taken together to comprise the baseline multivariate model. Next, the effect of adding lab serum measurements and PVAT biomarkers to the baseline features was measured for staging both advanced fibrosis and cirrhosis. Four multi-variate models were selected for further analysis: the best model without serum and PVAT measures, with serum measures and without PVAT measures, without serum measures and with PVAT measures, and with both serum measures and PVAT.

E. Statistical Analysis

To quantify the classification performance, AUC, sensitivity, and specificity were calculated. An AUC < 0.6 was considered an ineffective predictor. Youden's index was set as the threshold to compute specificity and sensitivity. The DeLong test (MLstatkit package, Python v.3.12) was used to compare the ROC curves from two models. A P-value < 0.05 was considered statistically significant.

III. RESULTS

A. Univariate Results

Table I describes the results from the univariate models. For cirrhosis, the spleen volume provided the highest AUC of 89.2% and specificity of 94.7%. However, the liver attenuation SD yielded a lower AUC of 66.5%, but the highest specificity of 98.7%. For advanced fibrosis, the FIB-4 serum score achieved the highest AUC of 83.2% and specificity of 86%. The spleen volume obtained a similar AUC of 82% and specificity of 82.5%. The liver attenuation SD achieved the highest specificity of 96.5% and the lowest AUC of 55.1%.

B. Multi-variate Results

Table I also describes the results from multi-variate models. Figure 2 shows ROC curves of the different multi-variate models for advanced fibrosis and cirrhosis.

Cirrhosis: The best multivariate features for cirrhosis (without serum or PVAT scores) included the spleen volume, LSVR, and volume proportions. The LR model with these features was termed the "baseline" model. It achieved a 91.6% AUC and 92.1% specificity for cirrhosis. Addition of the serum scores to the baseline model improved the AUC by 0.4% and specificity by 4%. Notably, addition of PVAT biomarkers to the baseline yielded the highest AUC of 96.3% and specificity of 97.4%. The PVAT biomarkers that were predictive included:
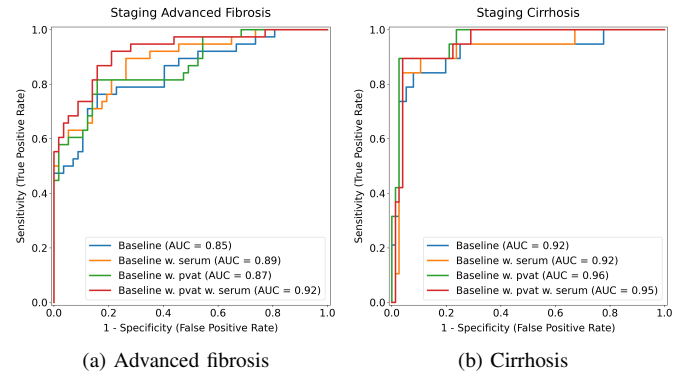

Fig. 2: ROC curves for staging advanced fibrosis (left) and cirrhosis (right) with logistic regression models.

(1) portal vein PVAT volume and fraction, (2) portal vein PVAT mean attenuation, (3) portal vein normalized and unnormalized SD attenuation, and (4) hepatic arteries PVAT fraction and normalized mean attenuation.

Addition of both PVAT and serum scores to the baseline model also improved its performance by 3.2% with a slight drop in specificity. The baseline model with PVAT (and the model with both PVAT and serum) was statistically significantly different (p < 0.05) compared to all the univariate models except spleen volume. However, statistical tests comparing the ROC curves from the different multivariate models yielded no significant differences for cirrhosis.

Advanced Fibrosis: For advanced fibrosis, the best baseline model used the spleen volume, LSVR, and LSN. It attained 84.7% AUC and 84.2% specificity, respectively. Addition of the serum scores to the baseline model improved the AUC by ∼4%, but the specificity dropped to 73.7%. Addition of the PVAT features further increased the AUC to 86.7% and the specificity remained the same at 84.2%. The PVAT scores included: (1) hepatic arteries PVAT normalized SD attenuation, (2) portal vein PVAT mean attenuation, (3) portal vein PVAT normalized and un-normalized SD sttenuation, and (4) PVAT fat fractions of the hepatic arteries and portal vein. Finally, the inclusion of both PVAT and serum biomarkers to the baseline model led to the highest AUC of 92.2% and specificity of 86%. This multivariate model was statistically significantly different (p < .05) from all univariate models and the baseline multivariate model with added serum scores.

IV. DISCUSSION

Our results are similar to prior work by Lee et al. [8], in which AUCs of 94% and 80% were obtained for cirrhosis and advanced fibrosis, respectively. In their work, biomarkers of the liver and spleen were derived from the respective segmentations and logistic regression models were also trained for staging advanced fibrosis and cirrhosis. Similarly, Lewis et al. [13] obtained AUCs of 92.5% and 83.8% for cirrhosis and advanced fibrosis, respectively. The latter approach also used explainable biomarkers for staging hepatic fibrosis, such as LSVR, spleen volume, and liver surface nodularity. A different

TABLE I: Results from the uni- and multi-variate logistic regression models trained to predict advanced fibrosis and cirrhosis. Blood serum scores (FIB-4 and APRI), Liver Segmental Volume Ratio (LSVR), Liver Surface Nodularity (LSN), Perivascular Adipose Tissue (PVAT), Portal Vein (PV), Hepatic Arteries (HA).

Model	Advanced Fibrosis			Cirrhosis		
	AUC (95% CI)	Sensitivity (95% CI)	Specificity (95% CI)	AUC (95% CI)	Sensitivity (95% CI)	Specificity (95% CI)
APRI	73.8 (62.0, 84.1)	55.3 (38.7, 71.1)	87.7 (78.0, 94.9)	82.3 (68.9, 93.0)	78.9 (58.3, 95.2)	84.2 (75.6, 92.0)
FIB4	83.2 (74.1, 91.6)	71.1 (55.8, 84.4)	86.0 (75.4, 94.6)	88.5 (78.0, 96.7)	73.7 (50.0, 91.7)	89.5 (82.2, 95.8)
Spleen Volume	82.0 (71.7, 90.9)	73.7 (59.4, 86.8)	82.5 (71.2, 91.4)	89.2 (77.1, 98.3)	78.9 (58.8, 95.2)	94.7 (88.9, 98.8)
Liver Attenuation SD	55.1 (41.4, 66.8)	26.3 (12.8, 40.0)	96.5 (91.1, 100.0)	66.5 (51.2, 81.5)	36.8 (16.7, 58.8)	98.7 (95.7, 100.0)
LSVR	73.5 (61.1, 82.9)	65.8 (50.0, 78.6)	77.2 (65.6, 87.0)	81.6 (71.0, 90.4)	84.2 (66.7, 100.0)	71.1 (60.5, 81.0)
LSN	76.3 (64.8, 86.7)	68.4 (52.9, 82.9)	80.7 (70.2, 91.2)	88.1 (79.9, 95.1)	84.2 (66.7, 100.0)	88.2 (80.3, 94.9)
PV PVAT Mean Atten.	58.0 (45.9, 70.2)	34.2 (18.7, 51.4)	84.2 (73.7, 92.9)	80.0 (68.6, 90.8)	57.9 (33.3, 82.4)	85.5 (76.6, 92.4)
PV PVAT Atten. SD	65.3 (54.4, 76.4)	97.4 (90.9, 100.0)	28.1 (17.0, 39.6)	81.4 (70.2, 91.5)	63.2 (41.2, 85.7)	86.8 (78.7, 93.8)
PV PVAT Fraction	46.2 (33.8, 58.8)	55.3 (39.0, 71.0)	52.6 (39.6, 65.5)	61.8 (48.5, 75.0)	68.4 (46.1, 88.9)	55.3 (43.9, 66.2)
PV PVAT Volume	44.1 (32.0, 56.5)	57.9 (42.4, 73.3)	50.9 (37.7, 64.2)	55.5 (42.3, 69.9)	73.7 (53.8, 93.8)	52.6 (41.3, 63.6)
HA PVAT Mean Atten.	72.3 (61.2, 82.1)	47.4 (32.4, 63.2)	89.5 (80.4, 96.5)	63.5 (47.3, 77.1)	42.1 (20.0, 64.3)	81.6 (72.2, 89.9)
HA PVAT Atten. SD	72.1 (60.8, 82.7)	81.6 (67.6, 92.9)	63.2 (50.9, 75.4)	63.4 (47.5, 77.4)	78.9 (58.8, 95.0)	48.7 (37.3, 60.0)
HA PVAT Fraction	60.3 (48.0, 72.2)	31.6 (17.6, 46.5)	91.2 (83.0, 98.0)	59.1 (41.0, 75.6)	42.1 (20.0, 64.3)	90.8 (83.5, 97.0)
HA PVAT Volume	48.4 (36.9, 59.9)	21.1 (8.6, 35.1)	87.7 (78.8, 95.2)	53.0 (36.3, 69.3)	31.6 (11.7, 52.6)	88.2 (80.6, 94.9)
Baseline	84.7 (75.5, 92.2)	76.3 (61.8, 89.2)	84.2 (73.4, 92.7)	91.6 (82.5, 98.4)	78.9 (58.8, 95.2)	92.1 (85.5, 97.4)
Baseline + serum	88.6 (81.0, 94.8)	89.5 (77.8, 97.6)	73.7 (61.4, 84.6)	92.0 (84.0, 98.7)	84.2 (66.7, 100.0)	96.1 (91.0, 100.0)
Baseline + PVAT	86.7 (78.7, 93.6)	78.9 (64.3, 91.4)	84.2 (73.6, 93.0)	96.3 (91.8, 99.3)	84.2 (65.0, 100.0)	97.4 (93.2, 100.0)
Baseline + PVAT + serum	92.2 (85.9, 97.3)	81.6 (69.2, 93.5)	86.0 (76.2, 94.5)	94.8 (89.3, 99.0)	84.2 (66.7, 100.0)	96.1 (91.0, 100.0)

deep learning algorithm [19] directly diagnosed the fibrosis stage, and yielded AUCs of 0.97 and 0.95 for distinguishing advanced fibrosis and cirrhosis, respectively. However, this approach required a large proprietary dataset of >7000 patients, and there are currently no public datasets available with confirmed fibrosis stages to replicate this work.

In contrast to these works, segmentations of hepatic arteries and portal vein were used to derive PVAT biomarkers for staging liver fibrosis. The PVAT-based biomarkers provided the greatest benefit for the advanced fibrosis stage. Notably, hepatic artery PVAT mean attenuation and SD showed the most potential in staging advanced fibrosis, and portal vein PVAT mean attenuation and SD showed the most potential in staging cirrhosis. Notably, this attests to the predictive capability of the PVAT biomarkers when added to the baseline multivariate model used for staging both cirrhosis and advanced fibrosis. Combining the PVAT biomarkers with serum scores, such as FIB4 and APRI, could potentially enhance the model performance even further [20], especially for advanced fibrosis.

These biomarkers used in this work are readily explainable and can be visually verified for consistency. This attests to the strength of our approach based on better descriptions of the biomarkers correlated with the disease. The results point to the deposition of fat surrounding vessels bound for the liver. The adipose tissue (AT) that accumulates in conditions like obesity can stimulate the development and progression of metabolic diseases such as cirrhosis and diabetes via multiple mechanisms. Visceral AT, for instance, causes an increase in fatty acids, glycerol, hormones, and inflammatory cytokines, and may lead to more severe conditions such as non-alcoholic steatohepatitis, cirrhosis, and hepatocellular carcinoma [21], [22]. PVAT can cause atherosclerosis via an "outside-in" theory: inflammatory mediators originating from PVAT travel to nearby vessels, cause vasoconstriction, and drive the genesis of atherosclerotic plaques [23]. It is unclear if this is due to an association with visceral fat accumulation and metabolic disorders, such as obesity, or if it is the result of an independent pathogenic response to liver disease [24].

There are limitations to our work. First, the approach was not evaluated on non-contrast CT and there was no validation on an external dataset. Furthermore, there were no statistical differences between the multivariate models for staging cirrhosis. But, this can be attributed to the small sample size (19 patients) used in this work for testing. External validation on more patients is paramount for the clinical translatability of this work, and it is the subject of future work. In summary, the non-invasive imaging-based biomarkers PVAT derived in this work were useful for staging advanced fibrosis and cirrhosis. The current approach shows promise for population-based studies of metabolic disease and opportunistic screening.

V. ACKNOWLEDGEMENTS

VI. COMPLIANCE WITH ETHICAL STANDARDS

This retrospective study using anonymized data did not require IRB approval.

REFERENCES

[1] Centers for Disease Control and Prevention, National Center for Health Statistics, "Chronic Liver Disease," Apr. 2024, accessed: 2024-08-05. [Online]. Available: https://www.cdc.gov/nchs/fastats/liver-disease.htm

[2] P. J. Pickhardt, K. Malecki, J. Kloke, and M. G. Lubner, "Accuracy of Liver Surface Nodularity Quantification on MDCT as a Noninvasive Biomarker for Staging Hepatic Fibrosis," *American Journal of Roentgenology*, vol. 207, no. 6, pp. 1194–1199, 2016.

[3] American Liver Foundation, "Fibrosis: Development," Jun. 2022, accessed: 2024-08-05. [Online]. Available: https://liverfoundation.org/about-your-liver/how-liver-diseases-progress/fibrosis-scarring/

[4] W. Im, J. Song, and W. Jang, "Noninvasive staging of liver fibrosis: review of current quantitative CT and MRI-based techniques," *Abdominal Radiology*, vol. 47, pp. 3051–3067, 2022.

[5] N. R. Mazumder, B. Enchakalody, P. Zhang, and G. Su, "Using Artificial Intelligence to Predict Cirrhosis From Computed Tomography Scans," *Clinical and Translational Gastroenterology*, vol. 14, no. 10, 2023.

[6] R. Sartoris, P.-E. Rautou, L. Elkrief, G. Pollorsi, F. Durand, D. Valla, L. Spahr, S. Terraz, O. Soubrane, F. Cauchy, V. Vilgrain, and M. Ronot, "Quantification of liver surface nodularity at ct: Utility for detection of portal hypertension," *Radiology*, vol. 289, no. 3, pp. 698–707, 2018, pMID: 30179109. [Online]. Available: https://doi.org/10.1148/radiol.2018181131

[7] Y. Yin, D. Yakar, R. A. J. O. Dierckx, K. B. Mouridsen, T. C. Kwee, and R. J. de Haas, "Liver fibrosis staging by deep learning: a visual-based explanation of diagnostic decisions of the model," *European Radiology*, vol. 31, no. 12, pp. 9620–9627, 2021.

[8] S. Lee, D. C. Elton, A. H. Yang *et al.*, "Fully Automated and Explainable Liver Segmental Volume Ratio and Spleen Segmentation at CT for Diagnosing Cirrhosis," *Radiology: Artificial Intelligence*, vol. 4, no. 5, p. e210268, 2022.

[9] P. J. Pickhardt, K. Malecki, C. B. O.F. Hunt, J. Kloke, T. Ziemlewicz, and M. G. Lubner, "Hepatosplenic volumetric assessment at MDCT for staging liver fibrosis," *European Radiology*, vol. 27, pp. 3060–3068, 2017.

[10] M. P. Diaz-Soto and G. Garcia-Tsao, "Management of varices and variceal hemorrhage in liver cirrhosis: a recent update," *Therapeutic Advances in Gastroenterology*, vol. 15, p. 17562848221101712, 2022, pMID: 35757384. [Online]. Available: https://doi.org/10.1177/17562848221101712

[11] T. S. Mathai, M. G. Lubner, P. J. Pickhardt, and R. M. Summers, "Fully Automated and Explainable Measurement of Liver Surface Nodularity in CT: Utility for Staging Hepatic Fibrosis ," *Academic Radiology*, vol. 1, no. 1, pp. 1–10, 2024.

[12] T. S. Mathai *et al.*, "Liver Surface Nodularity for Staging Hepatic Fibrosis on CT: A Comparative Study of Liver Segmenters," *Scientific Abstracts from the 2024 Conference on Machine Intelligence in Medical Imaging (CMIMI) of the Society for Imaging Informatics in Medicine (SIIM), Journal of Imaging Informatics in Medicine (Supplement)*, vol. 37, no. 1, pp. 1–35, 2024.

[13] S. V. Lewis, T. S. Mathai, M. G. Lubner, P. J. Pickhardt, and R. M. Summers, "Utility of Fully Automated Liver and Spleen Biomarkers for Staging Hepatic Fibrosis in CT," *Scientific Abstracts from the 2024 Conference on Machine Intelligence in Medical Imaging (CMIMI) of the Society for Imaging Informatics in Medicine (SIIM), Journal of Imaging Informatics in Medicine (Supplement)*, vol. 37, no. 1, pp. 1–35, 2024.

[14] J. Wasserthal, H.-C. Breit, M. T. Meyer, M. Pradella, D. Hinck, A. W. Sauter, T. Heye, D. T. Boll, J. Cyriac, S. Yang *et al.*, "Totalsegmentator: robust segmentation of 104 anatomic structures in ct images," *Radiology: Artificial Intelligence*, vol. 5, no. 5, 2023.

[15] M. Antonelli, A. Reinke *et al.*, "The medical segmentation decathlon," *Nat Commun*, vol. 13, no. 1, p. 4128, 2022.

[16] F. Isensee, P. F. Jaeger, S. A. Kohl, J. Petersen, and K. H. Maier-Hein, "nnu-net: a self-configuring method for deep learning-based biomedical image segmentation," *Nature methods*, vol. 18, no. 2, pp. 203–211, 2021.

[17] A. M. Nguyen, T. Sudharshan Mathai, L. Liu, J. Liu, and R. M. Summers, "Automated measurement of pericoronary adipose tissue attenuation and volume in ct angiography," in *2024 IEEE International Symposium on Biomedical Imaging (ISBI)*, 2024, pp. 1–5.

[18] D. Chatterjee, B. L. Shou, M. B. Matheson, M. R. Ostovaneh, C. Rochitte, M. Y. Chen, M. Dewey, J. Ortman, C. Cox, J. A. Lima, and A. Arbab-Zadeh, "Perivascular fat attenuation for predicting adverse cardiac events in stable patients undergoing invasive coronary angiography," *Journal of Cardiovascular Computed Tomography*, vol. 16, no. 6, pp. 483–490, 2022. [Online]. Available: https://www.sciencedirect.com/science/article/pii/S1934592522000727

[19] K. J. Choi, J. K. Jang, S. S. Lee, Y. S. Sung, W. H. Shim, H. S. Kim, J. Yun, J.-Y. Choi, Y. Lee, B.-K. Kang, J. H. Kim, S. Y. Kim, and E. S. Yu, "Development and validation of a deep learning system for staging liver fibrosis by using contrast agent–enhanced ct images in the liver," *Radiology*, vol. 289, no. 3, pp. 688–697, 2018, pMID: 30179104. [Online]. Available: https://doi.org/10.1148/radiol.2018180763

[20] Y.-H. Yen, F.-Y. Kuo, K.-M. Kee, K.-C. Chang, M.-C. Tsai, T.-H. Hu, S.-N. Lu, J.-H. Wang, C.-H. Hung, and C.-H. Chen, "Apri and fib-4 in the evaluation of liver fibrosis in chronic hepatitis c patients stratified by ast level," *PLOS ONE*, vol. 13, no. 6, pp. 1–16, 06 2018. [Online]. Available: https://doi.org/10.1371/journal.pone.0199760

[21] E. Lee, H. Korf, and A. Vidal-Puig, "An adipocentric perspective on the development and progression of non-alcoholic fatty liver disease," *Journal of Hepatology*, vol. 78, no. 5, pp. 1048–1062, 2023. [Online]. Available: https://www.sciencedirect.com/science/article/pii/S0168827823000776

[22] S. Dhokte and K. Czaja, "Visceral adipose tissue: The hidden culprit for type 2 diabetes," *Nutrients*, vol. 16, no. 7, 2024. [Online]. Available: https://www.mdpi.com/2072-6643/16/7/1015

[23] H. W. Kim, H. Shi, M. A. Winkler, R. Lee, and N. L. Weintraub, "Perivascular adipose tissue and vascular perturbation/atherosclerosis," *Arteriosclerosis, Thrombosis, and Vascular Biology*, vol. 40, no. 11, pp. 2569–2576, 2020. [Online]. Available: https://www.ahajournals.org/doi/abs/10.1161/ATVBAHA.120.312470

[24] O. W. Hamer, D. A. Aguirre, G. Casola, and C. B. Sirlin, "Imaging features of perivascular fatty infiltration of the liver: Initial observations," *Radiology*, vol. 237, no. 1, pp. 159–169, 2005, pMID: 16100085. [Online]. Available: https://doi.org/10.1148/radiol.2371041580